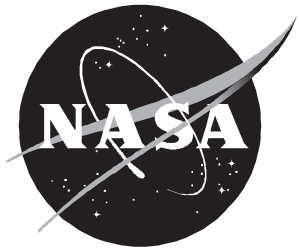

NASA Technical Memorandum 4656

Abrasion-Ablation Model for Neutron Production in Heavy Ion Reactions

Francis A. Cucinotta, John W. Wilson, and Lawrence W. Townsend

June 1995

NASA Technical Memorandum 4656

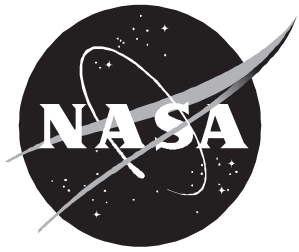

Abrasion-Ablation Model for Neutron Production in Heavy Ion Reactions

Francis A. Cucinotta, John W. Wilson, and Lawrence W. Townsend
Langley Research Center • Hampton, Virginia

National Aeronautics and Space Administration
Langley Research Center • Hampton, Virginia 23681-0001

June 1995

Available electronically at the following URL address: http://techreports.larc.nasa.gov/ltrs/ltrs.html

Printed copies available from the following:

NASA Center for AeroSpace Information
800 Elkridge Landing Road
Linthicum Heights, MD 21090-2934
(301) 621-0390

National Technical Information Service (NTIS)
5285 Port Royal Road
Springfield, VA 22161-2171
(703) 487-4650

Abstract

In heavy ion reactions, neutron production at forward angles is observed to occur with a Gaussian shape that is centered near the beam energy and extends to energies well above that of the beam. This paper presents an abrasion-ablation model for making quantitative predictions of the neutron spectrum. To describe neutrons produced from the abrasion step of the reaction where the projectile and target overlap, we use the Glauber model and include effects of final-state interactions. We then use the prefragment mass distribution from abrasion with a statistical evaporation model to estimate the neutron spectrum resulting from ablation. Measurements of neutron production from Ne and Nb beams are compared with calculations, and good agreement is found.

Introduction

Neutrons produced from the nuclear interactions of cosmic rays with the Earth's atmosphere, aircraft or spacecraft structural shielding, or the self-shielding of the human body are responsible for a large fraction of the energy deposition to passengers on high-altitude aircraft (ref. 1) and to astronauts in low Earth orbit. The nuclear reactions leading to the production of secondary neutrons from cosmic rays are dominated by the nucleon component; however, a significant fraction of neutrons are also produced in the interactions of the primary helium and heavy ion components of the cosmic rays with shielding. (See ref. 2.) Models of neutron production in heavy ion reactions are thus important inputs for the assessment of radiation damage from cosmic rays.

The study of neutron production from reactions induced by heavy ions may also present important insights into the theoretical modeling of the production of heavy fragments in these reactions. The abrasion-ablation model has been used for many years to describe mass yields in heavy ion collisions. (See refs. 3 to 6.) However, few attempts have been made to calculate nucleon production, including momentum distributions, in the abrasion-ablation model (ref. 7). Heavy ion fragment mass yields and nucleon production are ultimately related in these reactions, theoretically through the equations of motion or scattering amplitude. In references 8 and 9, measurements of inclusive neutron production in heavy ion collisions at 390*A* MeV and 800*A* MeV suggest that neutrons from the knockout stage of abrasion and the evaporation stage of ablation can be separated from the data. Madey and coworkers (refs. 8 and 9) have decomposed the neutron production data at forward angles into three Gaussian components of increasing widths. The narrowest component was attributed to evaporation neutrons, for which they found an effective temperature of around 2.7 MeV at 390*A* MeV and 3.3 MeV at 800*A* MeV. The second component of intermediate width was attributed to direct knockouts of neutrons. For this component, the width of the distribution was related to the internal momentum distribution of nucleons with Fermi momentum of about 250 MeV/*c*. The third and widest component was attributed to a high-momentum tail in the internal momentum distribution or to collective excitation effects. These results are useful because they suggest that some details of the different stages of the abrasion-ablation description can be uncovered from inclusive data where only the total distribution of neutrons is measured.

In this paper, we extend the abrasion-ablation model as formulated by Hüfner, Schäffer, and Schürmann to the evaluation of momentum distributions for nucleon production in heavy ion collisions (ref. 4). Using the Glauber model (ref. 10), we consider the spectrum of the knockouts in the overlap region of the collision. We also estimate the contribution of the final-state interactions of the knockouts for the projectile interacting with the prefragments. As in reference 4, the main approximations, other than the Glauber approximation, are derived from the treatment of the nuclear wave function, for which single-particle wave functions are used at all stages. In references 11 and 12, this formulation has been used to calculate proton production from ^{12}C and ^{40}Ar projectiles. Excitation energies from the abrasion stage are calculated in the geometric abrasion-ablation model (refs. 3 and 6) and used in the classical evaporation model (refs. 13 and 14) to estimate the neutron spectrum that originates in ablation. We then have a quantitative approach for considering the several mechanisms described in references 8 and 9 and can make comparisons that are consistent with the models describing heavy fragment yields.

The neutrons produced in the abrasion stage have momentum distributions largely determined by the ground-state, one-body density matrix of the projectile. To explain the high-momentum component of the neutron spectrum, we consider recent models that account for correlation effects based on calculations of the momentum distributions $n(\mathbf{p})$. (See refs. 15 and 16.) In many aspects, the physics of the calculations presented

here are similar to those contained in intranuclear cascade codes that use the Monte-Carlo method. (See refs. 17 and 18.) The formalism we present is useful first because of its simplicity because it involves only a few numerical integrations and second because of its ability to test nuclear structure inputs, such as the one-body density matrix. In the remainder of this paper, we first introduce the Glauber amplitude and recast the abrasion model in terms of the momentum distributions of the knockouts. The final-state interactions are then studied by correcting transition densities for rescattering effects. The energy spectrum of neutrons decaying from prefragments are then considered by using the classical evaporation model. Finally, we make comparisons with experiments and discuss the results of model calculations.

Symbols

A	mass number
B	two-body slope parameter, fm^2
$\mathbf{b}$	impact parameter, fm
c	speed of light, m/sec
E	energy, MeV
F	fragment
F^*	prefragment
F_l	probability of emission of ion l
f	scattering operator, fm
g_n	statistical weight
Im	imaginary part of function
$J_m^{(1)}$	cylindrical Bessel function of first kind of order m
K	projectile target relative wave number, fm^{-1}
$\mathbf{k}$	wave number of emitted neutrons, fm^{-3}
M	mass, MeV/c
m_N	nucleon mass, MeV/c^2
N_1	single-collision term
n	number of abraded nucleons
$n(\mathbf{p})$	momentum distribution
$n(\mathbf{x})$	Fourier transform of nucleon momentum distributions
P	projectile
$P(\mathbf{b}, \mathbf{b}')$	function describing projectile spectators
Q	defined in equation (13)
$\mathbf{q}$	momentum transfer, fm^{-3}
$\mathbf{r}$	internal nuclear coordinate, fm^3
S_n	separation energy, MeV
$\mathbf{s}$	transverse part of $\mathbf{r}$
T	target
w_0	level density of residual nucleus
X	final target state
z	component of $\mathbf{r}$
α	ratio of real to imaginary parts of f_{NN}
β	relative projectile target velocity
Γ	profile function
δ	Dirac delta function
ζ	target constituent
μ_n	neutron mass
ξ	defined in equation (22)
Λ_n	defined in equation (20)
$\rho(\mathbf{r})$	one-body density, fm^{-3}
$\rho(\mathbf{r}, \mathbf{r}')$	one-body density matrix, fm^{-3}
σ	cross section, mb
$\phi(\mathbf{r})$	single-particle wave function
χ	Eikonal phase
Ψ	complete nuclear wave function
Ω	Eikonal inelastic collision term

Subscripts:

abl	ablation
abr	abrasion
CN	formation cross section
f	final state
i	initial state
j	abraded nucleons (projectile constituents)
NN	nucleon-nucleon (two body)
P	projectile
T	target
X	final target state

Abrasion Theory

In the Glauber model the scattering operator for nucleus-nucleus collisions, as given in references 10 and 11, is

$$f = \frac{iK}{2\pi}\int d^2b\, \exp(i\mathbf{q}\cdot\mathbf{b})\,\Gamma(\mathbf{b}) \tag{1}$$

where K is the relative wave number of the projectile target, $\mathbf{b}$ is the impact parameter, and $\mathbf{q}$ is the momentum transfer. The profile function representing the multiple-scattering series at high energies is

$$\Gamma(\mathbf{b}) = 1 - \prod_{\zeta,j}\left[1 - \Gamma_{\zeta,j}(\mathbf{b} - \mathbf{s}_\alpha - \mathbf{s}_j)\right] \tag{2}$$

where ζ and j label the target and projectile constituents, respectively. In equation (2), $\Gamma_{\zeta,j}$ is the two-body profile function with the internal coordinate having components $\mathbf{r} = (\mathbf{s}, z)$.

The scattering amplitude of equation (1) is related to the production cross section for a projectile nucleon from the abrasion process by

$$\frac{d\sigma}{d\mathbf{k}} = \sum_X \frac{1}{(2\pi)^2}\int dE_{F^*} d^2q\, d^2b\, d^2b'\, \exp[i\mathbf{q}\cdot(\mathbf{b}-\mathbf{b}')]\,\delta(E_i - E_f)$$
$$\times \int \prod_{j=2}^{n}\left[\frac{d\mathbf{k}_j}{(2\pi)^3}\right]\langle TP|\Gamma^\dagger(\mathbf{b}')|XF^*\mathbf{k}_j\rangle\langle\mathbf{k}_j F^* X|\Gamma(\mathbf{b})|PT\rangle \tag{3}$$

where $\mathbf{k}_j$ denotes the wave numbers of the abraded nucleons, F^* denotes the prefragment (with $A_{F^*} = A_P - n$), and we have inserted initial and final states in equation (3).

The state dependence of the final target energy prevents closure on these states from being automatic in equation (3); however, when energy conservation is not considered, it is made outright (ref. 4). Next, we consider the change in energy of the target from the collision as follows:

$$E_T - E_X = E_T - \sqrt{(\mathbf{p}_T - \mathbf{q})^2 + M_X^2} = E_T\left(1 - \sqrt{1 + \frac{q^2 + M_X^2 - M_T^2}{E_T^2}}\right) \tag{4}$$

where M_T and M_X are the mass of the target in the initial and final states, respectively. We expect that performing closure on the $|X\rangle$ will be valid for sufficiently large values of E_T. After closure on the final target states, we find

$$\frac{d\sigma}{d\mathbf{k}} = \frac{1}{(2\pi)^2}\int dE_{F^*} d^2q\, d^2\mathbf{b}\, d^2\mathbf{b}'\, \exp[i\mathbf{q}\cdot(\mathbf{b}-\mathbf{b}')]\,\sigma_n\left(\mathbf{b}, \mathbf{b}', \mathbf{k}, \mathbf{q}, E_{F^*}\right) \tag{5}$$

where we define

$$\sigma_n\left(\mathbf{b}, \mathbf{b}', \mathbf{k}, \mathbf{q}, E_{F^*}\right) = \langle T|\left\{\int\prod_{j=2}^{n}\left[\frac{d\mathbf{k}_j}{(2\pi)^3}\right]\delta(E_i - E_f)\,\langle P|\Gamma^\dagger(\mathbf{b}')|F^*\mathbf{k}_j\rangle\langle\mathbf{k}_j F^*|\Gamma(\mathbf{b})|P\rangle\right\}|T\rangle \tag{6}$$

To consider the energy-conserving δ function in equation (6), we introduce the Fourier transform pair

$$\sigma_n(t) = \int dE\, \exp(-iEt)\,\sigma_n(E) \tag{7}$$

and

$$\sigma_n(E) = \int\frac{dt}{2\pi}\exp(iEt)\,\sigma_n(t) \tag{8}$$

In the projectile rest frame, we have

$$E_i - E_f = S_n - T_{F^*} + E_T - E_X - \sum_{j=1}^{n} \frac{\mathbf{k}_j^2}{2m_N} \tag{9}$$

where S_n is the separation energy and T_{F^*} is the recoil energy of the prefragment, including any excitation energy of the prefragments. We next go into temporal space to consider the $d\mathbf{k}_j$ integrals in equation (6) and thus rewrite equation (9) as

$$E_i - E_f = \bar{E} - \sum_{j=2} \frac{\mathbf{k}_j^2}{2m_N} \tag{10}$$

From equations (6), (7), and (10), we find

$$\sigma_n(t) = \langle T| \left\{ \int \prod_{j=2}^{n} \left[\frac{d\mathbf{k}_j}{(2\pi)^3} \right] \exp\left(-i \sum_{j=1} \frac{\mathbf{k}_j^2 t}{2m_N} \right) \langle P|\Gamma^\dagger(\mathbf{b}')|F^*\mathbf{k}_j\rangle \langle \mathbf{k}_j F^*|\Gamma(\mathbf{b})|P\rangle \right\} |T\rangle \tag{11}$$

To simplify equation (11), we first factor the profile function into projectile participant and spectator terms as

$$\Gamma(\mathbf{b}) = 1 - \prod_{l=n+1}^{A_P} Q_l(\mathbf{b} - \mathbf{s}_l) \prod_{j=1}^{n} Q_j(\mathbf{b} - \mathbf{s}_j) \tag{12}$$

where

$$Q_j = \prod_{\zeta=1}^{A_T} (1 - \Gamma_{\zeta,j}) \tag{13}$$

In the abrasion model, the orbits of the prefragments are assumed to be nearly the same as those of the projectile. This assumption is consistent with the use of the impulse and frozen nucleus approximations at high energies. A completely factored form in the participant and spectator coordinates is assumed for the projectile wave function

$$|P\rangle = |F\rangle|\phi_n\rangle \tag{14}$$

where $|F\rangle$ and $|\phi_n\rangle$ are the wave functions of the core (spectators) and of the knockouts (participants), respectively. The antisymmeterization is ignored in equation (14), which should be accurate if the mass of F is much larger than that of the knockouts. Antisymmeterization in the subsystems of $|F\rangle$ and $|\phi_n\rangle$ may still be included. By using plane-wave states for the $|\mathbf{k}_j\rangle$ and substituting equations (12) and (14) into equation (11), we find that

$$\begin{aligned} \sigma_n(t) = \langle T| \Bigg\{ & \binom{A_P}{n} \langle F| \prod_l Q_l^\dagger(\mathbf{b}' - \mathbf{s}_l')|F^*\rangle \langle F^*| \prod_l Q_l(\mathbf{b} - \mathbf{s}_l)|F\rangle \int d\mathbf{r}_1 d\mathbf{r}_1' \exp(i\mathbf{k}\cdot\mathbf{x}_1) Q_1^\dagger(\mathbf{b}' - \mathbf{s}_1') Q(\mathbf{b} - \mathbf{s}_1) \\ & \times \prod_{j=2}^{n} \left[\int \frac{d\mathbf{k}_j}{(2\pi)^3} d\mathbf{r}_j d\mathbf{r}_j' \exp(i\mathbf{k}_j\mathbf{x}_j) \exp\left(\frac{-k_j^2 t}{2m_N} \right) Q_j^\dagger(\mathbf{b}' - \mathbf{s}_j') Q_j(\mathbf{b} - \mathbf{s}_j) \right] \phi_n^\dagger(\mathbf{r}_1', \ldots, \mathbf{r}_n') \phi_n(\mathbf{r}_1, \ldots, \mathbf{r}_n) \Bigg\} |T\rangle \end{aligned} \tag{15}$$

where $\mathbf{x}_j = \mathbf{r}_j - \mathbf{r}_j'$. Using the coherent approximation for the target wave function in the intermediate states and the independent particle model for the fragment wave function leads to the following equation:

$$\sigma_n(t) = \binom{A_P}{n} P^{A_P - n}(\mathbf{b}, \mathbf{b}') \Lambda_{n-1}(\mathbf{b}, \mathbf{b}', t) \frac{dN_1}{d\mathbf{k}} \tag{16}$$

where the function $P(\mathbf{b}, \mathbf{b}')$ describes the projectile spectators as given by

$$P^{A_P - n}(\mathbf{b}, \mathbf{b}') = \langle TF | \prod_l Q_l^\dagger \left(\mathbf{b}' - \mathbf{s}_l' \right) | F^* \rangle \langle F^* | \prod_l Q_l (\mathbf{b} - \mathbf{s}_l) | FT \rangle \tag{17}$$

We next perform closure on the prefragments states in equation (17) because we do not consider coincidences with individual states. After closure we find that

$$P^{A_P}(\mathbf{b}, \mathbf{b}') = \langle TF | \prod_l Q_l^\dagger \left(\mathbf{b}' - \mathbf{s}_l' \right) Q_l (\mathbf{b} - \mathbf{s}_l) | FT \rangle \tag{18}$$

In equation (16) we have defined

$$\frac{dN_1}{d\mathbf{k}} = \frac{1}{(2\pi)^3} \int d\mathbf{r} d\mathbf{r}' \exp(i\mathbf{k} \cdot \mathbf{x}) \rho(\mathbf{r}, \mathbf{r}') Q_l^\dagger (\mathbf{b}' - \mathbf{s}') Q_l (\mathbf{b} - \mathbf{s}) \tag{19}$$

where $\rho(\mathbf{r}, \mathbf{r}')$ is the one-body density matrix of the projectile given by $\rho(\mathbf{r}, \mathbf{r}') = \phi^\dagger(\mathbf{r}') \phi(\mathbf{r})$. Next from equation (15), after evaluation of the integrals over $\mathbf{k}_j$ for $j > 2$, we find that

$$\Lambda_{n-1}(\mathbf{b}, \mathbf{b}', t) = \langle T | \int \prod_{j=2}^{n} \left[d\mathbf{r}_j d\mathbf{r}_j' \left(\frac{m_N}{2\pi i t} \right)^{3/2} \exp\left(\frac{-m_N x_j^2}{2it} \right) \rho\left(\mathbf{r}_j, \mathbf{r}_j' \right) Q_j^\dagger \left(\mathbf{b}' - \mathbf{s}_j' \right) Q_j (\mathbf{b} - \mathbf{s}_j) \right] | T \rangle \tag{20}$$

In energy space,

$$\begin{aligned} \Lambda_{n-1}\left(\mathbf{b}, \mathbf{b}', T_{F^*}, \mathbf{k} \right) = \langle T | \int \prod_{j=2}^{n} \left[d\mathbf{r}_j d\mathbf{r}_j' \rho\left(\mathbf{r}_j, \mathbf{r}_j' \right) Q_j^\dagger \left(\mathbf{b}' - \mathbf{s}_j' \right) Q_j (\mathbf{b} - \mathbf{s}_j) \right] \\ \times \frac{m_N}{2} \left(\frac{1}{2\pi} \right)^{3(n-1)/2} \frac{\xi_{n-1}^{[3(n-1)/2]-1}}{\bar{x}_{n-1}^{[3(n-1)/2]-1}} J^{(1)}_{[3(n-1)/2]-1} (\xi_{n-1} x_{n-1}) | T \rangle \end{aligned} \tag{21}$$

where $J_m^{(1)}$ is the cylindrical Bessel function of the first kind of order m and where

$$\xi_{n-1} = \sqrt{2m_N \left[T_{F^*} + \frac{\mathbf{k}^2}{2m_N} - S_n - (E_T - E_X) \right]} \tag{22}$$

and

$$\bar{x}_{n-1} = \sqrt{\sum_{j=2}^{n} x_j^2} \tag{23}$$

For $n = 1$, we have $\Lambda_0 = \delta(T_{F^*})$. If we assume forward-peaked density matrices (about), a small argument expansion of the Bessel functions can be developed (ref. 11) that results in

$$\Lambda_{n-1}\left(\mathbf{b}, \mathbf{b}', T_{F^*}, \mathbf{k} \right) \approx C_{n-1} \left[T_{F^*} + \frac{\mathbf{k}^2}{2m_N} - S_n - (E_T - E_X) \right]^{(n-1)} \Lambda_1^{n-1} \left(\mathbf{b}, \mathbf{b}', \frac{\xi_{n-1}}{\sqrt{n-1}} \right) + O(\xi^4 x^4) \tag{24}$$

where, for example, $C_1 = 1$, $C_2 = \frac{\pi}{4}$, $C_3 = \frac{\pi}{105}$, and $C_4 = \frac{\pi^2}{204}$.

The nucleon momentum distribution from abrasion then takes the following form:

$$\left(\frac{d\sigma}{d\mathbf{k}} \right)_{\text{abr}} = \sum_n \binom{A_P}{n} \frac{1}{(2\pi)^2} \int d^2q d^2b d^2b' \exp[iq \cdot (\mathbf{b} - \mathbf{b}')] P^{A_P - n}(\mathbf{b}, \mathbf{b}') \frac{dN_1}{d\mathbf{k}} \int dT_{F^*} \Lambda_{n-1}\left(\mathbf{b}, \mathbf{b}', T_{F^*}, \mathbf{k} \right) \tag{25}$$

If

$$q^2 + M_T^2 - M_X^2 \ll E_T^2 \tag{26}$$

we may approximate equation (25) as

$$\left(\frac{d\sigma}{d\mathbf{k}}\right)_{\text{abr}} \approx \sum_n \binom{A_P}{n} \int d^2b P^{A_P - n}(\mathbf{b}) \frac{dN_1}{d\mathbf{k}} \int dT_{F^*} \Lambda_{n-1}(\mathbf{b}, T_{F^*}, \mathbf{k}) \tag{27}$$

The result of equation (27) suggests that for $A_P \gg 1$, the momentum dependence of higher production terms $(n > 1)$ should be similar to that of the leading-order terms. (See appendix.) This result supports the success of the hard-scattering model of Hatch and Koonin (ref. 19), which only uses the single-scattering mechanism to predict the shape of the inclusive proton distribution in heavy ion collisions. The model developed here differs from the hard-scattering model by our use of the target closure approximation. In this approximation, the effects of smearing of the secondary momentum from the target knockouts are not considered. Instead, these effects are replaced by averages represented by the target density and by using only on-shell, two-body amplitudes. Also, the Glauber model has a much fuller multiple-scattering structure than does the hard-scattering model.

To include the effects of final-state interactions of the nucleon knockouts, we use the Eikonal model described in reference 11. In this model, the plane waves are replaced by the distorted wave for the nucleon-projectile recoil interaction evaluated at the relative energy between the knockout and the recoil. Modifying equation (19) as in reference 11 gives

$$\frac{dN_1}{d\mathbf{k}} = \frac{1}{(2\pi)^3} \int d\mathbf{r} d\mathbf{r}' \exp(i\mathbf{k} \cdot \mathbf{x}) \rho(\mathbf{r}, \mathbf{r}') \exp[-2Im\chi^{(-)}(y)] Q_l^\dagger(\mathbf{b}' - \mathbf{s}') Q_l(\mathbf{b} - \mathbf{s}) \tag{28}$$

where $\chi^{(-)}$ is the outgoing Eikonal phase. Equation (28) ignores off-shell effects but includes the energy dependence of the final-state interaction and assumes a medium modified interaction, as described in reference 11.

Optical Limit for Profile Functions

For $A_P A_T \gg 1$, the optical limit of the profile functions occurring in the previous equations may be used (refs. 10 and 20). From reference 20, we find in the optical limit that

$$P^{A_P}(\mathbf{b}, \mathbf{b}') = \exp\{i[\chi(\mathbf{b}) - \chi^\dagger(\mathbf{b}')]\} \tag{29}$$

where the Eikonal phase is

$$\chi(\mathbf{b}) = \frac{A_P A_T}{(2\pi k_{NN})} \int d^2q \exp(i\mathbf{q} \cdot \mathbf{b}) F_P(q) F_T(q) f_{NN}(q) \tag{30}$$

with $F(q)$ denoting the one-body form factor and f_{NN} denoting the two-body scattering amplitude, which we represent by

$$f_{NN} = \frac{\sigma_{NN}(\alpha + i) k_{NN}}{4\pi} \exp\left(\frac{-1}{2} B q^2\right) \tag{31}$$

where σ_{NN} is the two-body total cross section, k_{NN} is the relative momentum in two-body center of mass frame, B the two-body slope parameter, and α the ratio of the real to imaginary parts of $f_{NN}(\mathbf{q} = 0)$. For the inelastic terms, we write in the optical limit (ref. 20) that

$$Q_j^\dagger\left(\mathbf{b}' - \mathbf{s}_j'\right) Q_j(\mathbf{b} - \mathbf{s}_j) = \exp\left[\tilde{\Omega}\left(\mathbf{b}' - \mathbf{s}_j', \mathbf{b} - \mathbf{s}_j\right)\right] - 1 \tag{32}$$

with

$$\tilde{\Omega}\left(\mathbf{b}' - \mathbf{s}_j', \mathbf{b} - \mathbf{s}_j\right) = \frac{1}{(2\pi k_{NN})^2} \sum_\alpha \int d^2q d^2q' \exp[i\mathbf{q} \cdot (\mathbf{b} - \mathbf{s}_j + \mathbf{s}_\alpha)] \exp\left[-i\mathbf{q} \cdot \left(\mathbf{b}' - \mathbf{s}_j' + \mathbf{s}_\alpha\right)\right] f_{NN}^\dagger(\mathbf{q}') f_{NN}(\mathbf{q}) \tag{33}$$

Model for Nuclear Density Matrix

We next describe a local density approximation for the one-body density matrix. For a projectile nucleus, the one-body density matrix is defined in terms of the complete nuclear wave function Ψ (ref. 15) as follows:

$$\rho(\mathbf{r}, \mathbf{r}') = \int d\mathbf{r}_2\, d\mathbf{r}_3 \ldots d\mathbf{r}_{A_P} \Psi^{\dagger}\left(\mathbf{r}', \mathbf{r}_2, \ldots, \mathbf{r}_{A_P}\right)\Psi\left(\mathbf{r}, \mathbf{r}_2, \ldots, \mathbf{r}_{A_P}\right) \tag{34}$$

Evaluation of equation (34) requires knowledge of the complete nuclear wave function; however, in practice a model is introduced. In the Fermi gas model, the density matrix is represented as

$$\rho(\mathbf{r}, \mathbf{r}') = \rho_o \frac{3j_1\left(k_F|\mathbf{r}-\mathbf{r}'|\right)}{k_F|\mathbf{r}-\mathbf{r}'|} \tag{35}$$

where k_F is the Fermi momentum and ρ_o is the density of nuclear matter. The Fermi gas model is known to provide a poor representation of the density matrix. However, its form suggests the use of a local density model, for which the density matrix is assumed to factor as

$$\rho(\mathbf{r}, \mathbf{r}') \approx \rho(\mathbf{y})\, n(\mathbf{x}) \tag{36}$$

with $\mathbf{x} = \mathbf{r} - \mathbf{r}'$ and $\mathbf{y} = \frac{1}{2}(\mathbf{r} + \mathbf{r}')$ and where the one-body density is given by the diagonal part of the density matrix

$$\rho(\mathbf{r}) \approx \rho(\mathbf{r}, \mathbf{r}') \qquad (\mathbf{r}' = \mathbf{r}) \tag{37}$$

and $n(\mathbf{x})$ is the Fourier transform of the nucleon momentum distribution

$$n(\mathbf{x}) = \int d\mathbf{p} \exp(i\mathbf{p} \cdot \mathbf{x})\, n(\mathbf{p}) \tag{38}$$

where $n(\mathbf{p})$ is defined by

$$n(\mathbf{p}) = \int d\mathbf{r} d\mathbf{r}' \exp(-i\mathbf{p} \cdot \mathbf{x})\, \rho(\mathbf{r}, \mathbf{r}') \tag{39}$$

with normalization

$$\int n(\mathbf{p}) \frac{d\mathbf{p}}{(2\pi)^3} = 1 \tag{40}$$

The one-body density is reasonably well known from elastic electron scattering. The nucleon momentum distribution at small to modest values of p is known from inclusive inelastic electron scattering. For large p values, backward production of protons suggests that large enhancements to the nucleon momentum distribution result from correlation effects when compared with predictions of independent-particle models. In addition, this enhancement is largely independent of nuclear mass.

Haneishi and Fujita (ref. 21) have introduced the following momentum distribution:

$$n(\mathbf{p}) = n_0 \sum_{i=1}^{3} C_i \exp\left(-\frac{p^2}{2p_i^2}\right) \tag{41}$$

where n_0 is a normalization constant. The last term in equation (41) is expected to directly reflect the nuclear correlations. The value of $C_3 = 0.003$, used in reference 21, was based on estimates from backwards proton production. This value was found to be too large in references 11 and 12; thus, the value $C_3 = 0.0008$ is used herein. In equation (41), p_1 is related to the Fermi momentum by $p_1 = \sqrt{2/5}k_F$. Values for k_F are listed in table 1, and the other parameters of equation (41) are listed in table 2. Figure 1 compares the model of equation (39) with a Fermi gas model that includes only the first term in equation (41) and with the correlation model of reference 16.

Table 1. Experimental Determination of Fermi Momentum for Several Nuclei

Nucleus	k_F, MeV/c
^{12}C	184
^{20}Ne	230
^{40}Ar	240
^{93}Nb	255
^{197}Au	265

Table 2. Parameters for Momentum Distribution Model of Equation (41)

i	p_i, MeV/c	C_i
1	$\sqrt{2/5}k_F$	1
2	$\sqrt{6/5}k_F$	.03
3	500	0.0008

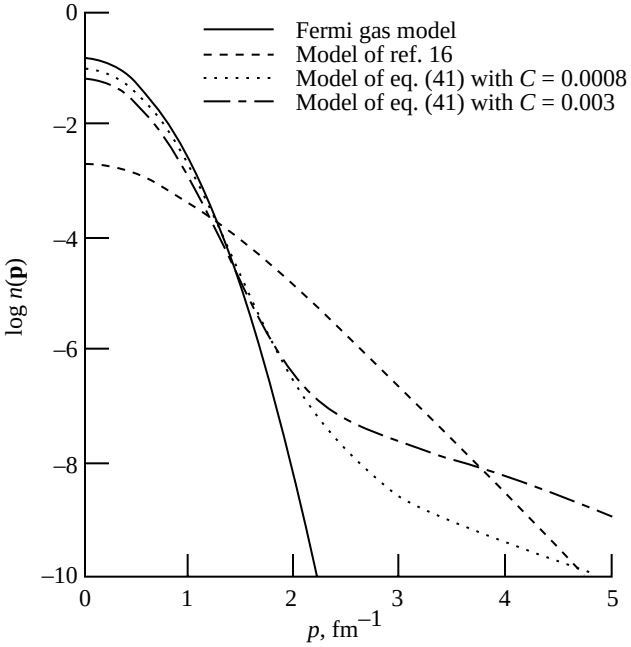

Figure 1. Internal nucleon momentum distribution for Ne versus momentum for several models.

Neutron Spectrum From Ablation

After the projectile-target collision, a distribution of prefragment nuclei in states of excitation remain. The excitation spectrum is treated as an average state in the abrasion-ablation model, with a single or small number of average excitation energies used to describe the prefragment and the strength of the state determined by the total abrasion cross section. A microscopic formulation of nucleon and cluster abrasion describes transitions to individual levels of the prefragment nuclei (ref. 22). Here we follow the approach described in references 3 and 6 for estimating average excitation energies and calculate the neutron spectrum from ablation with the Weisskopf-Ewing statistical decay model. We define $P_n(j, \mathbf{k})$ as the probability that a prefragment labeled j with mass number A_j, charge number Z_j, and excitation energy E_j^*, emits a neutron of momentum $\mathbf{k}$ (refs. 13 and 14). The momentum distribution for neutron production from ablation in the projectile rest frame is written as

$$\left(\frac{d\sigma}{d\mathbf{k}}\right)_{\text{abl}} = \sum_j \sigma_{\text{abr}}\left(A_j, Z_j, E_j^*\right) P_n(j, \mathbf{k}) \qquad (42)$$

The total abrasion cross section in equation (42) is evaluated from the abrasion momentum distribution in equation (27), as discussed in the appendix.

In the statistical model, the prefragment (compound nucleus) is assumed to be infinitely heavy, and the emission spectrum is assumed to be isotropic in the rest frame. The probability function, as given in references 13 and 14, is

$$P_n(j, E_n) = \frac{2\mu_n g_n E_n \sigma_{CN} w_o\left(E_j^* - E_n\right)}{\sum_l F_l} \qquad (43)$$

where μ_n is the neutron mass, g_n is the statistical weight, σ_{CN} is the formation cross section by the inverse process, and w_o is the level density of the residual nucleus. In equation (43) we have

$$F_l = \int_0^{E_l^* - S_j} P_l(j, E)\, dE \qquad (44)$$

We consider competition between the emission of the light particles n, p, d, t, h, and α. The model parameters are taken from Dostrovsky (ref. 23). If sufficient excitation energy is available, then several neutrons will be emitted. We then evaluate the cumulative spectrum as

$$P_n(j, E_n) = P_n(j, E_n) + \sum_l \int_0^{E_j^*} P_l(j, E_l)\, P_n(k, E_n)\, dE_l + \ldots \qquad (45)$$

In this work, terms through the third order in the series of equation (45) are considered. The neutron momentum distribution in the lab frame is found by multiplying equation (42) by the neutron energy to form a Lorentz invariant and then performing the transformation to the laboratory system.

Results for Forward Neutron Production

The production of secondary neutrons from 390*A* MeV and 800*A* MeV ^{20}Ne and ^{93}Nb beams has been measured in the forward direction with targets of NaF and Pb (refs. 8 and 9). In figures 2 to 4, we compare these data with calculations based on the previous formalism. For calculations, the NaF target is represented by ^{20}Ne. The measurements are for the inclusive production of neutrons, and the calculations shown consider the neutron production from the target nuclei in the knockout stage of abrasion. For the Nb projectile, some underestimation of the evaporation peak centered at the beam energy (fig. 4) occurred and may be due to the inclusion of only up to third-order terms in the evaporation chain. The underestimation of the evaporation peak for the ^{93}Nb beam may not be of concern for cosmic ray studies for which Fe is usually the heaviest ion of interest.

The high-energy component of neutrons extends well above the velocity corresponding to that of the projectile beam. As discussed previously, in predicting inclusive proton yields (ref. 12), model calculations are only successful in predicting the high-energy component of the spectrum when the internal nucleon momentum

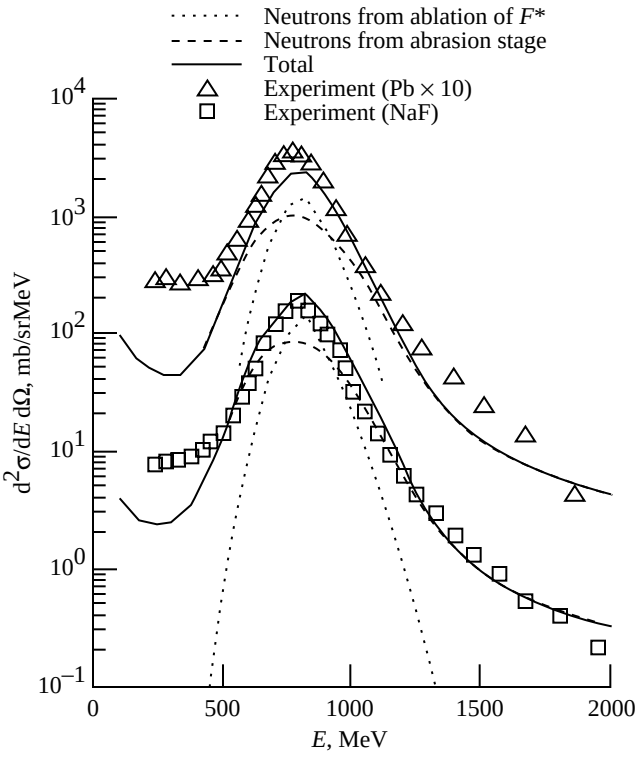

Figure 3. Calculations versus experimental data (from refs. 8 and 9) for energy spectrum of secondary neutrons at 0° in laboratory for Ne beams at 800*A* MeV colliding with NaF and Pb targets.

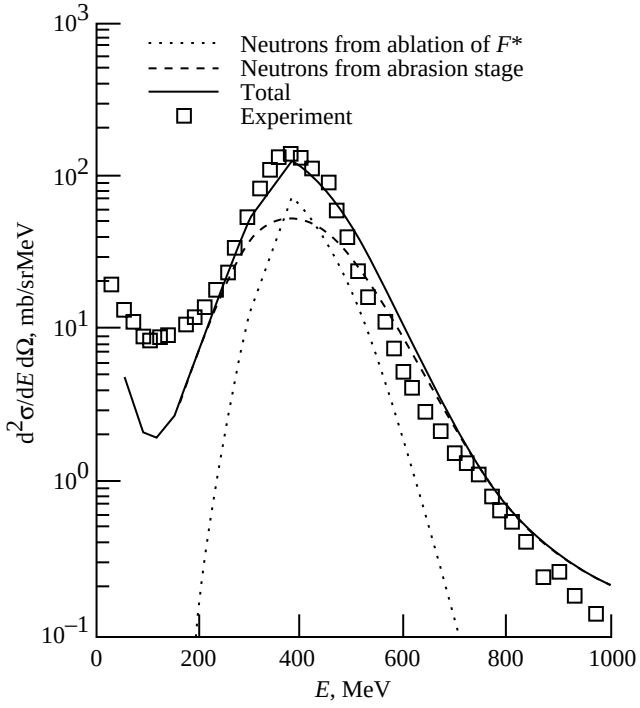

Figure 2. Calculations versus experimental data (from refs. 8 and 9) for energy spectrum of secondary neutrons at 0° in laboratory for Ne beams at 390*A* MeV colliding with NaF targets.

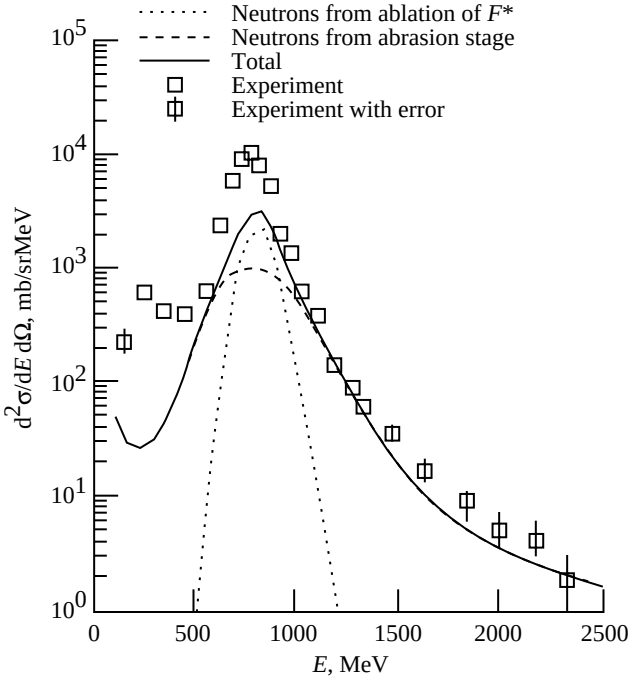

Figure 4. Calculations versus experimental data (from refs. 8 and 9) for energy spectrum of secondary neutrons at 0° in laboratory for Nb beams at 800*A* MeV colliding with Nb targets.

spectrum contains correlation effects. Here the Fermi gas model underestimates the data by several orders of magnitude. The dependence on the target mass of the high-energy component (fig. 3) indicates that multiple scattering also affects this component. The model calculations do not account for higher order cascade effects of projectile knockouts interacting with the projectile prefragments (other than the overall absorption). The calculations also do not account for the production of nucleons through the decay of nucleon isobars that are produced in the reaction. Both of these contributions are important for energies intermediate between that of the initial beam and target and grow in importance with the angle of production. Calculations of these processes will be discussed in future work.

Concluding Remarks

The production of secondary neutrons in heavy ion collisions has been formulated with the two-stage abrasion-ablation model. Good agreement with experimental data for forward neutron production is found. Calculations show that neutrons produced in both stages of the reaction are important. The secondary neutrons produced in nuclear abrasion extend to velocities well above that of the beam velocity in these reactions. This extension is a result of correlation effects that occur in the internal nucleon momentum distribution and through multiple scattering. The results of these calculations will be used to develop databases for cosmic ray shielding studies.

Appendix

Kinematical Phase Space and Inclusive Momentum Distribution

In this appendix, we discuss the relationship of the multiple-production terms of nucleons abraded from the projectile to the kinematical phase space. We also consider an approximation with the Glauber multiple-scattering series, in which energy conservation is ignored entirely.

The scattering amplitude for the heavy ion collision is related to the cross section by the phase space of each particle that appears in the final state. We consider inclusive reactions in which a nucleon originating in the projectile is measured. For simplicity, the final target state is not considered, and we use closure on these states with a single momentum vector denoted by $\mathbf{p}_X$ to represent these states. The cross section is then determined by

$$d\sigma = \frac{(2\pi)^4}{\beta}\sum_X d\mathbf{p}_X d\mathbf{p}_{F^*}\sum_{n=1}\prod_{j=1}^{n}[d\mathbf{p}_j] \times \delta(E_i - E_f)\,\delta(\mathbf{p}_i - \mathbf{p}_f)\,|T_{fi}|^2 \quad \text{(A1)}$$

where β is the relative projectile target velocity, F^* represents the prefragments, n is the number of nucleons knocked out of the projectile in the overlap region with the target, and i and f denote the initial and final states, respectively. The prefragment decays through particle emission when sufficient energy is available. To include the phase space of decay products of F^*, we write

$$d\mathbf{p}_{F^*} = d\mathbf{p}_F\prod_{r=0} d\mathbf{p}_r \quad \text{(A2)}$$

where r denotes the ions (if any) emitted in ablation. To consider nucleon production from ablation, we would study the $\mathbf{p}_r$. We use the momentum-conserving δ function in equation (A1) to eliminate $\mathbf{p}_F$ from equation (A1).

We next consider using energy conservation in equation (A1). Working in the projectile rest frame, we transform $d\mathbf{p}_X$ to $d\mathbf{q}$, where $\mathbf{q} = \mathbf{p}_T - \mathbf{p}_X$ is the total momentum transfer in the collision and use the energy-conserving δ function in equation (A1) to eliminate dq_L where q_L is the longitudinal momentum transfer. We then find

$$d\sigma = (2\pi)^4\sum_X d\mathbf{q}_T K\prod_{r=0}[d\mathbf{p}_r]\sum_{n=1}\prod_{j=1}^{n}[d\mathbf{q}_j]\,|T_{fi}|^2 \quad \text{(A3)}$$

where the phase space factor is defined as

$$K = \frac{1}{\beta}\frac{-\partial E_f}{\partial q_L} = \frac{1}{\beta}\frac{E_X E_{F^*}}{E_{F^*}(p_T - q_L) + E_X\left(\sum_j p_j\cos\theta_j - q_L\right)} \quad \text{(A4)}$$

The momentum distribution of nucleons from abrasion is then given as

$$\frac{d\sigma}{d\mathbf{p}} = (2\pi)^4\sum_X\int d\mathbf{q}_T\sum_{n=1}\int\prod_{j=2}^{n}d\mathbf{p}_j\prod_{r=0}d\mathbf{p}_r K|T_{fi}|^2 \quad \text{(A5)}$$

Equation () corresponds closely to equation (3) if we make the following replacement:

$$K = \int dq_L\,\delta(E_i - E_f) \rightarrow \int dE_{F^*}\,\delta(E_i - E_f) \quad \text{(A6)}$$

If energy conservation is ignored entirely, then we would have $K = 1$. When the participant-spectator arrangement of the Glauber series previously discussed is used, the inclusive momentum distribution becomes

$$\frac{d\sigma}{d\mathbf{k}} = \sum_n\binom{A_P}{n}\int d^2bP^{A_P - n}(\mathbf{b})\frac{dN_n}{d\mathbf{k}} \quad \text{(A7)}$$

where

$$\frac{dN_n}{d\mathbf{k}} = \frac{dN_1}{d\mathbf{k}}[1 - P(\mathbf{b})]^{n-1} \quad \text{(A8)}$$

and note that

$$\int\frac{dN_1}{d\mathbf{k}}d\mathbf{k} = 1 - P(\mathbf{b}) \quad \text{(A9)}$$

The result of equation (A8) indicates that the inclusive momentum distribution from abrasion essentially follows the shape of the leading-order term in the approximations discussed because since the absorptive factors in equation (A7) change slowly with increasing n for $A_P \gg 1$. The total cross section for abrading n nucleons follows from equations (A7) through (A9) as

$$\sigma_n = \binom{A_P}{n}\int d^2bP^{A_P - n}(\mathbf{b})\,[1 - P(\mathbf{b})]^n \quad \text{(A10)}$$

which is in agreement with references 4 or 5.

References

1. Reitz, G.: Radiation Environment in the Stratosphere. *Radiat. Prot. Dosim.*, vol. 48, no. 1, 1993, pp. 5–20.

2. Cucinotta, Francis A.: *Calculations of Cosmic-Ray Helium Transport in Shielding Materials.* NASA TP-3354, 1993.

3. Bowman, J. D.; Swiatecki, W. J.; and Tsang, C. F.: *Abrasion and Ablation of Heavy Ions.* LBL-2908, Univ. of California, July 1973.

4. Hüfner, J.; Schäfer, K.; and Schürmann, B.: Abrasion-Ablation in Reactions Between Relativistic Heavy Ions. *Phys. Rev. C*, vol. 12, no. 6, Dec. 1975, pp. 1888–1898.

5. Townsend, L. W.; Wilson, J. W.; Cucinotta, F. A.; and Norbury, J. W.: Comparison of Abrasion Model Differences in Heavy Ion Fragmentation—Optical Versus Geometric Models. *Phys. Rev. C*, vol. 34, no. 4, Oct. 1986, pp. 1491–1494.

6. Wilson, John W.; Townsend, Lawrence W.; and Badavi, F. F.: A Semiempirical Nuclear Fragmentation Model. *Nucl. Instrum. & Methods Phys. Res.*, vol. B18, no. 3, Feb. 1987, pp. 225–231.

7. Hüfner, J.; and Nemes, M. C.: Relativistic Heavy Ions Measure the Momentum Distribution on the Nuclear Surface. *Phys. Rev. C*, vol. 23, no. 6, June 1981, pp. 2538–2547.

8. Madey, R.; Varga, J.; Baldwin, A. R.; Anderson, B. D.; Cecil, R. A.; Fai, G.; Tandy, P. C.; and Watson, J. W.: Inclusive Neutron Spectra at 0° From the Reactions Pb(Ne,*n*)*X* and NaF*(*Ne,*n)X* at 390 and 790 MeV per Nucleon. *Phys. Rev. Lett.*, vol. 55, no. 14, Sept. 1985, pp. 1453–1456.

9. Madey, R.; Zhang, W. M.; Anderson, B. D.; Baldwin, A. R.; Flanders, B. S.; Pairsuwan, W.; Varga, J.; and Watson, J. W.: Inclusive Neutron Spectra at 0° From Nb-Nb and Au-Au Collisions at 800 MeV/Nucleon. *Phys. Rev. C*, vol. 38, no. 1, July 1988, pp. 184–194.

10. Glauber, R. J.; and Matthiae, G.: High-Energy Scattering of Protons by Nuclei. *Nucl. Phys.*, vol. B21, no. 1, Aug. 1, 1970, pp. 135–157.

11. Cucinotta, Francis A.: *Multiple-Scattering Model for Inclusive Proton Production In Heavy Ion Collisions*. NASA TP-3470, 1994.

12. Cucinotta, Francis A.: Forward Production of Protons in Relativistic ^{12}C-Nucleus Collisions. *J. Phys. G: Nucl. Part. Phys.*, vol. 20, 1994, pp. 1803–1815.

13. Weisskopf, V. F.; and Ewing, D. H.: On the Yield of Nuclear Reactions With Heavy Elements. *Phys. Rev.*, vol. 57, Mar. 15, 1940, pp. 472–485.

14. Kikuchi, Ken; and Kawai, Mitsuji: *Nuclear Matter and Nuclear Reactions*. John Wiley & Sons, Inc., 1968.

15. Antonov, A. N.; Hodgson, P. E.; and Petkov, I. Zh.: *Nucleon Momentum and Density Distributions in Nuclei.* Oxford Univ. Press, 1988.

16. Amado, R. D.; and Woloshyn, R. M.: Mechanism for 180° Proton Production in Energetic Proton-Nucleus Collisions. *Phys. Rev. Lett.*, vol. 36, no. 24, June 14, 1976, pp. 1435–1440.

17. Cugnon, J.: Monte Carlo Calculation of High-Energy Heavy-Ion Interactions. *Phys. Rev. C*, vol. 22, no. 5, Nov. 1980, pp. 1885–1896.

18. Yariv, Y.; and Fraenkel, Z.: Intranuclear Cascade Calculation of High-Energy Heavy-Ion Interactions. *Phys. Rev. C*, vol. 20, no. 6, Dec. 1979, pp. 2227–2243.

19. Hatch, R. L.; and Koonin, S. E.: High Momentum Nucleons From Relativistic Nuclear Collisions. *Phys. Lett.*, vol. 81B, no. 1, Jan. 29, 1979, pp. 1–4.

20. Cucinotta, Francis A.; Townsend, Lawrence W.; and Wilson, John W.: Inclusive Inelastic Scattering of Heavy Ions in the Independent Particle Model. *J. Phys. G.: Nucl. Part. Phys.*, vol. 18, no. 5, May 1992, pp. 889–901.

21. Haneishi, Y.; and Fujita, T.: Problem of Backward Proton Production. *Phys. Rev. C*, vol. 33, no. 1, Jan. 1986, pp. 260–274.

22. Cucinotta, Francis A.; and Dubey, Rajendra R.: Alpha-Cluster Description of Excitation Energies in ^{12}C(^{12}C,3 α)*X* at 2.1*A* GeV. *Phys. Rev. C*, vol. 50, no. 2, Aug. 1994, pp. 1090–1096.

23. Dostrovsky, I.; Fraenkel, Z.; and Friedlander, G.: Monte Carlo Calculations of Nuclear Evaporation Processes. III. Applications to Low-Energy Reactions. *Phys. Rev.*, vol. 116, no. 3, Nov. 1, 1959, pp. 638–702.

REPORT DOCUMENTATION PAGE

Form Approved
OMB No. 0704-0188

1. AGENCY USE ONLY *(Leave blank)*	2. REPORT DATE	3. REPORT TYPE AND DATES COVERED
	June 1995	Technical Memorandum

4. TITLE AND SUBTITLE
Abrasion-Ablation Model for Neutron Production in Heavy Ion Reactions

5. FUNDING NUMBERS
WU 199-45-16-12

6. AUTHOR(S)
Francis A. Cucinotta, John W. Wilson, and Lawrence W. Townsend

7. PERFORMING ORGANZATION NAME(S) AND ADDRESS(ES)
NASA Langley Research Center
Hampton, VA 23681-0001

8. PERFORMING ORGANIZATION REPORT NUMBER
L-17455

9. SPONSORING/MONITORING AGENCY NAME(S) AND ADDRESS(ES)
National Aeronautics and Space Administration
Washington, DC 20546-0001

10. SPONSORING/MONITORING AGENCY REPORT NUMBER
NASA TM-4656

11. SUPPLEMENTARY NOTES

12a. DISTRIBUTION/AVAILABILITY STATEMENT
Unclassified–Unlimited
Subject Category 73
Availability: NASA CASI (301) 621-0390

12b. DISTRIBUTION CODE

13. ABSTRACT *(Maximum 200 words)*

In heavy ion reactions, neutron production at forward angles is observed to occur with a Gaussian shape that is centered near the beam energy and extends to energies well above that of the beam. This paper presents an abrasion-ablation model for making quantitative predictions of the neutron spectrum. To describe neutrons produced from the abrasion step of the reaction where the projectile and target overlap, we use the Glauber model and include effects of final-state interactions. We then use the prefragment mass distribution from abrasion with a statistical evaporation model to estimate the neutron spectrum resulting from ablation. Measurements of neutron production from Ne and Nb beams are compared with calculations, and good agreement is found.

14. SUBJECT TERMS	15. NUMBER OF PAGES
Galactic cosmic rays; Radiation protection; Secondary neutrons; High-altitude aircraft	13
	16. PRICE CODE: A03

17. SECURITY CLASSIFICATION OF REPORT	18. SECURITY CLASSIFICATION OF THIS PAGE	19. SECURITY CLASSIFICATION OF ABSTRACT	20. LIMITATION OF ABSTRACT
Unclassified	Unclassified	Unclassified	

National Aeronautics and
Space Administration
Langley Research Center
Mail Code 180
Hampton, VA 23681-0001